Interconnection of renewable sources : Multi-Active-Bridge Converter

Abdennour Merrouche, Thierry Talbert, Daniel Matt, Thierry Martiré, Guillaume Pellecuer

Interconnection of renewable sources : Multi-Active-Bridge Converter

Abdennour Merrouche
PROMES-CNRS, Perpignan University Via Domitia
IES, Montpellier University
Perpignan, Montpellier, France
abdennour.merrouche@promes.cnrs.fr

Thierry Talbert
PROMES-CNRS, Perpignan University Via Domitia
Perpignan, France
thierry.talbert@promes.cnrs.fr

Daniel Matt
IES, Montpellier University
Montpellier, France
daniel.matt@umontpellier.fr

Thierry Martiré
IES, Montpellier University
Montpellier, France
thierry.martire@umontpellier.fr

Guillaume Pellecuer
IES, Montpellier University
Montpellier, France
guillaume.pellecuer@umontpellier.fr

***Abstract*—This article presents the design of a three-port, three-phase Multi-Active Bridge converter. This converter aims to interconnect various renewable energy sources with electrical loads, using hydrogen as an energy storage medium for domestic applications. Photovoltaic panels will serve as the primary energy source; any excess energy produced will be stored as hydrogen using an electrolyzer. When the photovoltaic panels are unable to meet consumption needs, electrical energy will be generated from the stored hydrogen using a fuel cell. The Multi-Active Bridge consists of three three-phase inverters magnetically coupled through a transformer. The objective of this converter is to regulate the energy flow among the different components of the structure, operating through a 'phase-shift' control method applied between the three inverters.**

***Index Terms*—Multi-Active Bridge, phase-shift, hydrogen, photovoltaïc.**

I. Introduction

Renewable energies play a crucial role in limiting climate change caused by the use of fossil fuels, the primary source of CO_2 emissions. Renewable energies have limitations in their utilization, with the primary one being their intermittent nature, thus requiring a system capable of energy storage. In the case of a photovoltaic installation, batteries offer an intriguing solution due to their high efficiencies, reaching up to 90% for certain technologies like lithium-ion. Despite the batteries' good performance, they only provide a medium-term solution. Hydrogen could be an interesting option for long-term storage due to its physical properties [1]. There are various methods for hydrogen production; however, the method considered the least polluting involves using renewable energies to power an electrolyzer, thereby producing what is termed as "green" hydrogen. The objective of this article is to present a three-phase three-port Multi-Active-Bridge converter. This converter aims to interconnect multiple energy sources as well as electrical loads [2][3]. Additionally, the transformer provides galvanic isolation between these different energy sources [4][5]. In this context, the structure includes photovoltaic panels, an electrolyzer, and a fuel cell.

Funded by Labex SOLSTICE. This work is supported by the French program "Investissements d'avenir" managed by the National Research Agency (ANR) under the contract ANR-10-LABX-22-01.

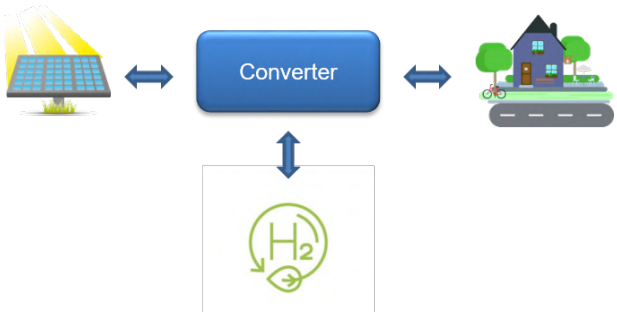

Fig. 1. Diagram of the multi-source system.

As shown in Fig. 1, the implemented system will operate as follows: electricity will be generated by photovoltaic panels. This energy will then be stored as hydrogen using an electrolyzer. Subsequently, the hydrogen will be converted back into electricity via a fuel cell when the photovoltaic panels cease producing energy. RTE France Annual Electrical Report 2020, along with the simulation software Pvsyst, allows estimating the electrical production for the average annual consumption of a household of 4 people, with a 9 kW photovoltaic installation located in the region of Perpignan. This estimation highlights two significant aspects: higher consumption during the winter period and an overproduction of photovoltaic energy during the summer. This overproduction represents a considerable potential as it can be stored in the form of hydrogen, offering the prospect of achieving an annual energy self-sufficiency of 105%.

II. Multi-Active-Bridge Converter

A proof of concept has been achieved by combining three energy sources using a dedicated converter designed for this purpose. The electrical circuit diagram, in Fig. 2, the sources

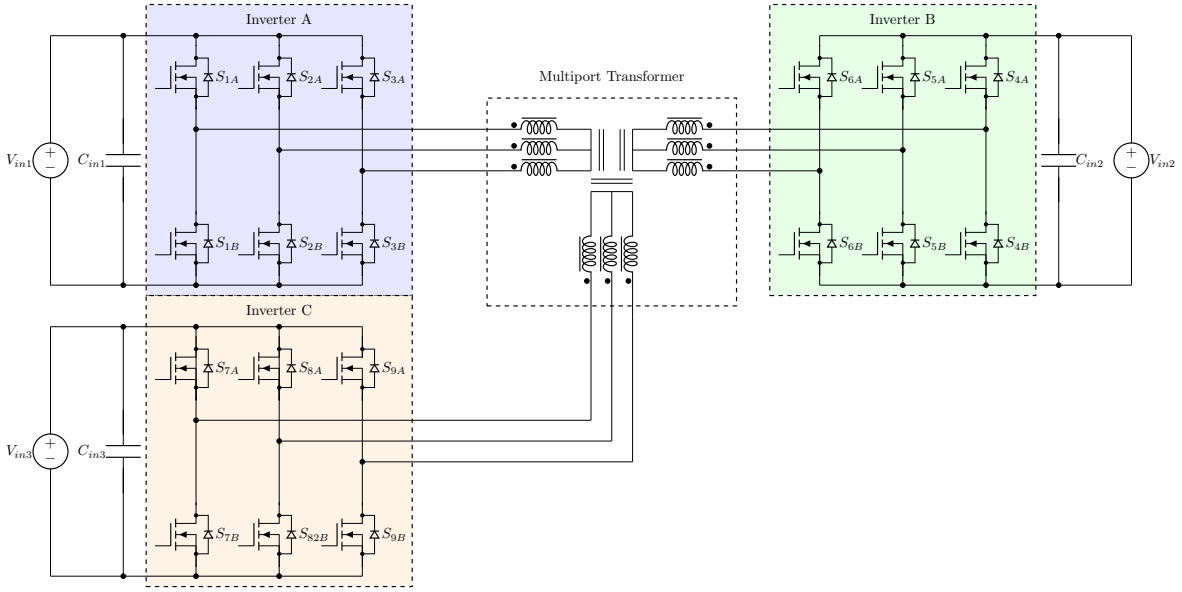

Fig. 2. Electrical diagram of the Multi-Active-Bridge. Composed of 3 three-phase inverters (A)(B)(C) and a Multi-port transformer.

are connected through three-phase inverters and a transformer acting as a coupling element, specifically designed for the application. Each inverter generates a magnetic flux within the transformer. When balanced, the magnetic fluxes from the 3 inverters cancel each other out, resulting in no power exchange. By adjusting the control of the inverters to manipulate the phase difference between the control commands, we can create a magnetic imbalance and transfer energy from one source to another. This is the principle behind "phase-shift" control.

III. Modeling and Sizing of the Transformer

A. Theoretical model

The transformer is the key component of the converter. Its realization requires precise modeling and dimensioning. Each system (inverter + transformer) can be represented by an equivalent impedance, allowing the calculation of the required phase shift for each inverter to control energy exchanges. This representation must account for the self and mutual inductances of each phase and each inverter. Fig. 3

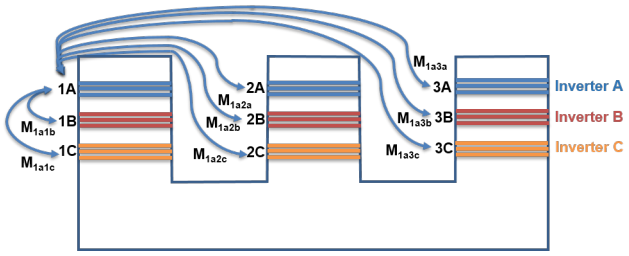

Fig. 3. Representation of the self and mutual inductance of phase 1 of inverter A.

displays the mutual inductances of phase 1 of inverter A. This representation can be applied to each phase and each inverter of the converter. The transformer can be modeled by a 9x9 inductance matrix (1) representing the self and mutual inductances of each winding of every inverter. This allows the extraction of important parameters such as the magnetizing inductance, the leakage inductances, and the power exchanged depending on the phase shift between the inverters.

$$\begin{pmatrix} L_{1a} & M_{1a2a} & M_{1a3a} & \dots & M_{1a3c} \\ M_{2a1a} & L_{2a} & M_{2a3a} & \dots & M_{2a3c} \\ M_{3a1a} & M_{3a2a} & L_{3a} & \dots & M_{3a3c} \\ \vdots & \vdots & \vdots & \ddots & \vdots \\ M_{3c1a} & M_{3c2a} & M_{3c3a} & \dots & L_{3c} \end{pmatrix} \quad (1)$$

with L representing the self inductance and M the mutual inductance.

In [6], it was demonstrated that this new matrix allows linking the magnetizing inductance and the leakage inductances of the system. In [7][8], an N-branch transformer can be represented by an equivalent T-model, as shown in Fig. 4, with N+1 inductances.

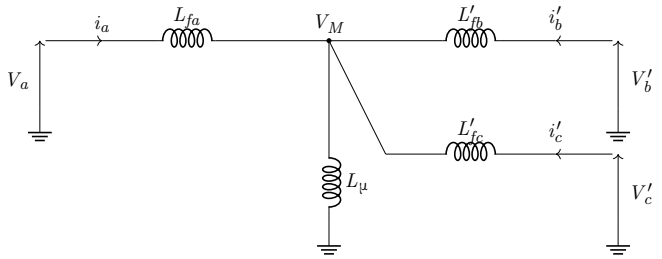

Fig. 4. T-model of the transformer.

L_f represents the Leakage inductance and L_μ the Magnetizing inductance. If we consider the equivalent T-model, taking phase 1 of each inverter as a reference, it is possible to quickly calculate the power supplied by the three energy sources.

$$K_{ab} = \frac{V_b}{V_a} = \frac{i_a}{i_b} = \frac{M_{C_{bc}}}{M_{C_{ac}}} \tag{2}$$

$$K_{ac} = \frac{V_c}{V_a} = \frac{i_a}{i_c} = \frac{M_{C_{bc}}}{M_{C_{ab}}} \tag{3}$$

$$L_\mu = \frac{M_{C_{ac}}.M_{C_{ab}}}{M_{C_{bc}}} \tag{4}$$

$$L_{fa} = L_{C_a} - \frac{M_{C_{ac}}.M_{C_{ab}}}{M_{C_{bc}}} \tag{5}$$

$$L'_{fb} = \frac{L_{C_b} - \frac{M_{C_{ab}}.M_{C_{bc}}}{M_{C_{ac}}}}{K_{ab}^2} \tag{6}$$

$$L'_{fc} = \frac{L_{C_c} - \frac{M_{C_{ac}}.M_{C_{bc}}}{M_{C_{ab}}}}{K_{ac}^2} \tag{7}$$

L_C represents the Cyclic self-inductance considers the interaction between the self-inductance and the mutual inductances within the same inverter. M_C represents the Cyclic mutual inductance considers the effect between the mutual inductances within the same leg and those of the same inverter. V_M represents the midpoint potential, V_a is the input voltage of inverter A and serves as a reference. V_b and V_c are the input voltages of inverters B and C, respectively phased by angles φ_{ab} and φ_{ac} relative to V_a. ($V_a = [V_m; 0°]$,$V_b = [V_m; \varphi_{ab}]$,$V_c = [V_m; \varphi_{ac}]$). From this, the expressions (7), (8) and (9) are obtained [6][9].

$$P_a = -\frac{3V_m^2.(\frac{sin(\varphi_{ab})}{L'_{fb}} + \frac{sin(\varphi_{ac})}{L'_{fc}})}{2L_{fa}.w.\alpha} \tag{8}$$

$$P_b = -\frac{3V_m^2.(\frac{sin(\varphi_{ab})}{L'_{fb}} + \frac{sin(\varphi_{ac})}{L'_{fc}} - sin(\varphi_{ab}).\alpha)}{2L'_{fb}.w.\alpha} \tag{9}$$

$$P_c = -\frac{3V_m^2.(\frac{sin(\varphi_{ab})}{L'_{fb}} + \frac{sin(\varphi_{ac})}{L'_{fc}} - sin(\varphi_{ac}).\alpha)}{2L'_{fc}.w.\alpha} \tag{10}$$

With $\alpha = (\frac{1}{L_\mu} + \frac{1}{L_{fa}} + \frac{1}{L'_{fb}} + \frac{1}{L'_{fc}})$.
The convention used to express power exchanges between the inverters indicates that when power is negative, the source absorbs power, and when it is positive, it supplies power. Therefore, by adjusting the phase shift of the inverter controls, it is possible to manage power transfer.

B. Finite Element Sizing

The COMSOL software allows for the realization of a 3D electromagnetic modeling of the transformer using the finite element method Fig. 5. This modeling and simulation confirmed the theoretical sizing by incorporating a Jiles-Artheton magnetic model, thereby validating the energy exchange principle between inverters through the ”phase shift” control. Fig. 5 shows the magnetic induction in the transformer for a voltage of 33V and a frequency of 50kHz. The simulation results demonstrate that the expected powers are achieved without causing saturation of the magnetic core, thereby confirming the ability to transfer power between the inverters. Using

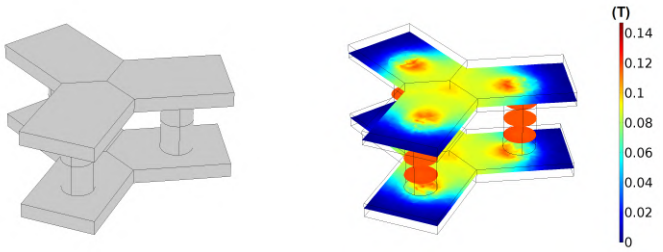

Fig. 5. 3D Electromagnetic Simulation of Magnetic Induction in the Transformer.

electromagnetic simulation, it is possible to determine the theoretical inductance matrix. From the inductance matrix, it is possible to express the magnetic coupling coefficients k_{xy}, with M the mutual inductance and L the self inductance.

$$k_{xy} = \frac{M_{xy}}{\sqrt{L_x L_y}} \tag{11}$$

Subsequently, with the help of LTspice software, it will be possible to simulate and compare the magnetic coupling model with its equivalent T-model. The results in Fig. 6 indicate that

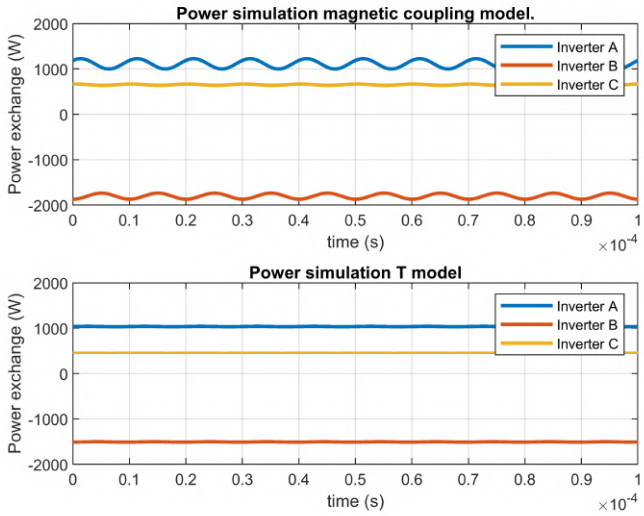

Fig. 6. Simulation combining magnetic coupling model and T-model.

the two models show differences because, in the T model, the leakage inductances of the three inverters are considered equivalent for the same phase. In reality, implementing a multiport transformer with equal leakage inductances is a complex task, and as a result, the outcomes can significantly vary. Since the theoretical expressions are derived from the T-model, the results obtained from equations (7), (8), and (9) correspond to those obtained from simulating the T-model.

IV. Experimental Test Result of the Converter

As shown in Fig. 7, the manufactured transformer features two 3C90 magnetic cores that can be stacked. The windings for each inverter are placed on PCBs arranged to overlap within the three ’legs’.

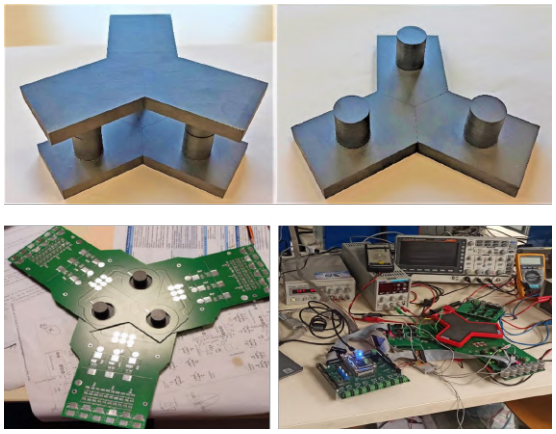

Fig. 7. Prototype of the Three-Port Three-Phase Multi-Active Bridge Converter.

The control of each inverter operates in full-wave mode for a supply voltage V_{in} = 20 V and a switching frequency of 50 kHz.

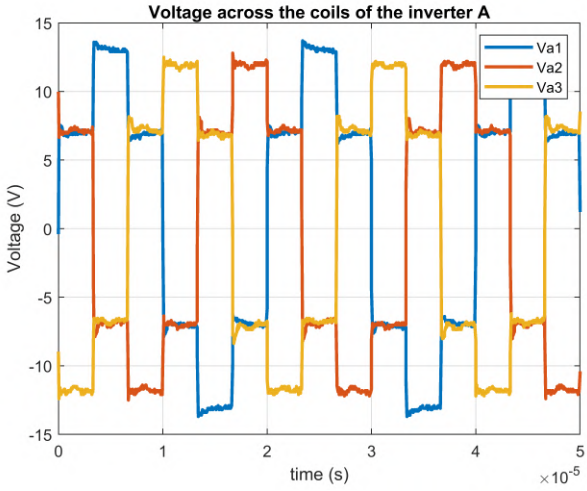

Fig. 8. Input voltage of the transformer.

Fig. 8 shows the voltages across the three phases at the terminals of inverter A.

$$V_{max} = \frac{2}{3}.V_{in} \tag{12}$$

The equation (12) represents the theoretical maximum value of the voltage across the coils when the inverter operates in full-wave mode, with V_{max} as the peak voltage across the coils and V_{in} as the input voltage of the inverter.

Fig. 9 shows the currents in the coils of inverter A when the phase shifts ϕ_{ab} and ϕ_{ac} are at 0°. Currents ripples are present due to the leakage and magnetizing inductances of the transformer.

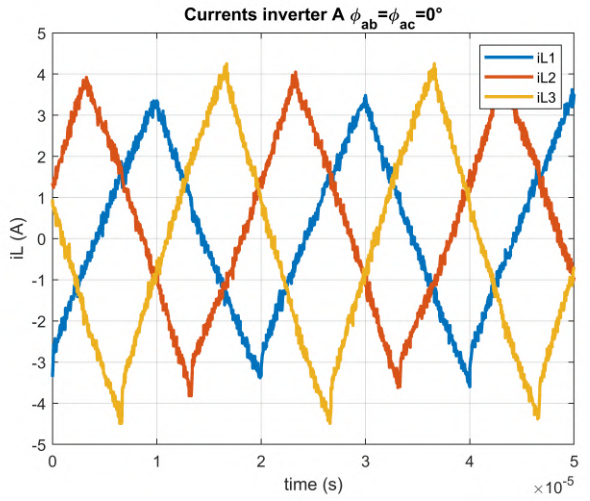

Fig. 9. Currents of the inverter A $\phi_{ab} = \phi_{ac}$=0°.

The magnetic flux in each branch of the transformer is shown in Fig. 10.

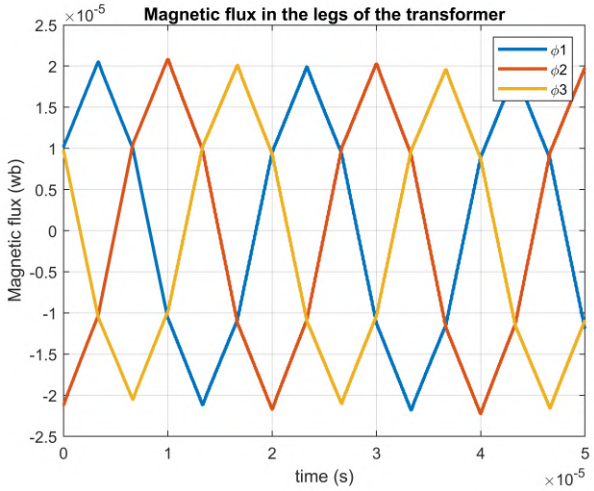

Fig. 10. Magnetic flux in the legs of the transformer.

Fig. 11 depicts the maximum currents for each inverter, with phase shifts ranging from -10° to 13°. Each inverter is set up with a specific phase shift combination to reach its peak current. For inverter A, this current is highest when ϕ_{ab} and ϕ_{ac} are both at -10°. In the case of inverter B, it peaks at ϕ_{ab} = 13° and ϕ_{ac} = 10°. For inverter C, the current peaks at ϕ_{ab} = -10° and ϕ_{ac} = 13°. Despite the 50 kHz switching frequency, the presence of significant currents for small phase shifts is due to the lack of series inductances. The Multi-Active-Bridge relies solely on the low values of leakage and magnetizing inductances of the transformer, typically in the microhenry range.

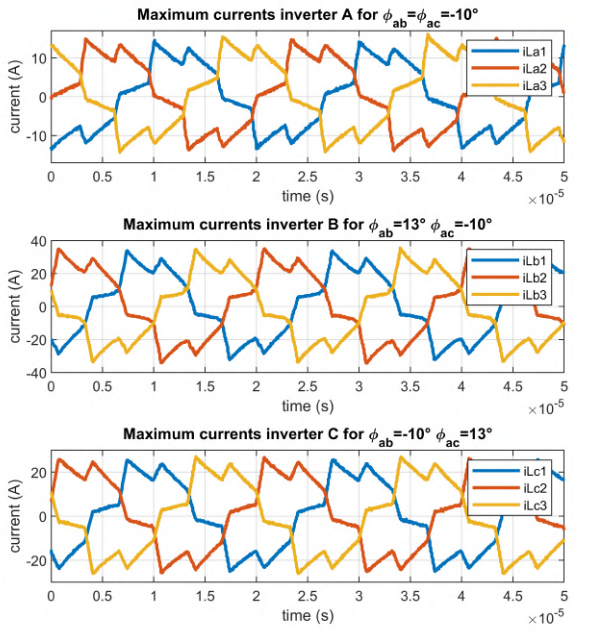

Fig. 11. Maximum current for each inverter.

For the same operating conditions, with V_{in}=20 V and switching frequency f=50 kHz, we can graphically represent the evolution of exchanged powers based on the phase shift angles ϕ_{ab} and ϕ_{ac}.

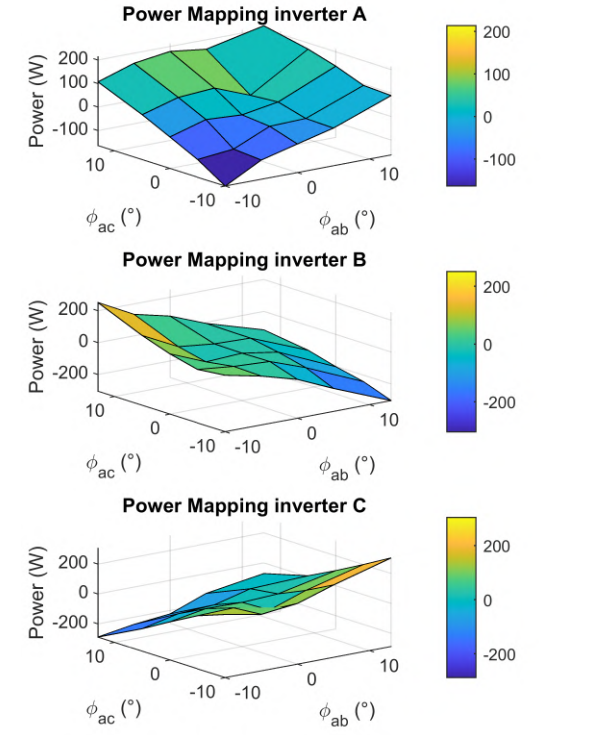

Fig. 12. Experimental Power Mapping of the Multi-Active Bridge Converter.

Fig. 12 shows that the power mapping of the converter validates the operating principle of the Multi-Active Bridge and demonstrates the ability to control energy exchange between different sources by adjusting the phase shift between the inverters.

V. Conclusion

This study focuses on the development of a three-phase Multi-Active Bridge converter aimed at interconnecting various renewable energy sources using hydrogen as a storage medium. Theoretical analysis has shed light on the possibility of energy exchange among different sources through a specific 'phase shift' control. Initial results from experimental tests have validated the theoretical and simulation work, showcasing the feasibility of such a converter.

VI. Acknowledgement

I would like to thank Labex Solstice for funding the work presented in this article.

References

[1] WILDGRUBER, Otto. Hydrogen as energy source : an introduction. Energy & Environment, 2006, vol. 17, no 2, p. 275-279.

[2] FALCONES, Sixifo, AYYANAR, Rajapandian, et MAO, Xiaolin. A DC–DC multiport-converter-based solid-state transformer integrating distributed generation and storage. IEEE Transactions on Power electronics, 2012, vol. 28, no 5, p. 2192-2203.

[3] CHEN, Yenan, WANG, Ping, LI, Haoran, et al. Power flow control in multi-active-bridge converters: Theories and applications. In : 2019 IEEE Applied Power Electronics Conference and Exposition (APEC). IEEE, 2019. p. 1500-1507.

[4] GALESHI, Soleiman, FREY, David, et LEMBEYE, Yves. Efficient and scalable power control in multi-port active-bridge converters. In : 2020 22nd European Conference on Power Electronics and Applications (EPE'20 ECCE Europe). IEEE, 2020. p. P. 1-P. 9.

[5] YANG, Jiajun, BUTICCHI, Giampaolo, GU, Chunyang, et al. A generalized input impedance model of multiple active bridge converter. IEEE Transactions on Transportation Electrification PP(99).

[6] G. Pellecuer, T. Martire, M. Petit and B. Loyer, "On-Board Power Management in a Marine Autonomous Surface Vehicle (ASV): Multi-Port Transformer Design," PCIM Europe 2022; International Exhibition and Conference for Power Electronics, Intelligent Motion, Renewable Energy and Energy Management, Nuremberg, Germany, 2022, pp. 1-9, doi: 10.30420/565822275.

[7] C. Sun, N. H. Kutkut, D. W. Novotny, et D. M. Divan, " General equivalent circuit of a multiwinding co-axial winding transformer ", in IAS '95. Conference Record of the 1995 IEEE Industry Applications Conference Thirtieth IAS Annual Meeting, 1995, vol. 3, p. 2507-2514 vol.3. doi: 10.1109/IAS.1995.530622.

[8] H. Tao, A. Kotsopoulos, J. L. Duarte and M. A. M. Hendrix, "A Soft-Switched Three-Port Bidirectional Converter for Fuel Cell and Supercapacitor Applications," 2005 IEEE 36th Power Electronics Specialists Conference, 2005, pp. 2487-2493,doi: 10.1109/PESC.2005.15819

[9] M. Neubert, R.W. De Doncker, J. Biela, "Modeling, Synthesis and Operation of Multiport-Active Bridge Converters", Universitätsbibliothek der RWTH Aachen, 2020.